

1 **Fill dynamics and sample mixing in the AirCore**

2 **Pieter P. Tans**

3 **Global Monitoring Laboratory, National Oceanic and Atmospheric Administration**

4 **325 Broadway, Boulder, CO 80305**

5

6 **Abstract**

7 The AirCore is a long coiled tube that acts as a “tape recorder” of the composition of air as it is  
8 slowly filled or flushed. When launched by balloon with one end of the tube open and the other  
9 closed, the initial fill air flows out during ascent as the outside air pressure drops. During descent  
10 atmospheric air flows back in. I We describe how we can associate the position of an air parcel  
11 in the tube with the altitude it came from by modeling the dynamics of the fill process. The  
12 conditions that need to be satisfied for the model to be accurate are derived. The extent of mixing  
13 of air parcels that enter at different times is calculated, so that we know how many independent  
14 samples are in the tube upon landing, and later when the AirCore is analyzed.

15

16 **1. Introduction**

17 When the Aircore is filling with atmospheric air coming in through the open end the newly  
18 sampled air pushes the air that is already in the tube deeper into the tube while compressing it.  
19 This mode of sampling is entirely passive, relying on the pressure continuing to increase as the  
20 altitude becomes lower during descent. The AirCore could also be flushed by a pump without  
21 any need for pressure changes of the outside air that is being sampled. I conceived the idea of  
22 AirCore in the late 1990s after we had found ~100 year old air, as indicated by the measured  
23 levels of CO<sub>2</sub> and CH<sub>4</sub>, near the bottom of the firn layer at a depth of ~90 m at the South Pole  
24 (Battle, 1996). The air was very old despite the fact that there was still open contact with the  
25 present-day atmosphere. Over distances of tens of meters or more molecular diffusion is  
26 exceedingly slow! The root-mean-square (rms) molecular diffusion distance is  $X_{rms} = (2Dt)^{0.5}$ . D  
27 is diffusivity in air, for CO<sub>2</sub> it is 0.140 cm<sup>2</sup> s<sup>-1</sup> at 1 bar and 0 degree C, t is time in seconds. After  
28 one year the rms diffusion distance for CO<sub>2</sub> in air would be ~30 m which would be the scale of  
29 spreading if there is no macroscopic air motion at all. In addition, diffusive mixingity deep in the  
30 firn is significantly slower than in open air because the air path from the bottom of the firn to the  
31 atmosphere has many detours going through the pores that are still open.

32 With Jim Smith and Michael Hahn, two members of our group in those days, we verified that  
33 there is very little mixing along the length of the tube by pushing slugs of air from two different  
34 reference air cylinders, alternating between high and low CO<sub>2</sub>, through a long coiled tube. We

35 also stored air for several hours before analysis. It all looked good. Then we tried a balloon  
36 flight. In order to make the payload lighter we switched from stainless steel to aluminum tubing,  
37 because of our excellent experience with long term gas storage in high pressure aluminum  
38 cylinders. It did not work at all. The easily bendable tube was made of a soft aluminum alloy,  
39 very different from the high pressure cylinders. We found that the tube ~~consumed made~~-CO<sub>2</sub>  
40 ~~disappear~~ very effectively. It was going to take more effort to make it successful, and we did not  
41 have much time to devote to it. So the project languished for several years until Anna Karion,  
42 Colm Sweeney, and Tim Newberger of our group at GML were able to pick it up again. At the  
43 urging of Sandy MacDonald, who was director of NOAA's Earth System Research Laboratory at  
44 the time, I applied for a patent in August 2006. He pointed out that there are people trolling the  
45 scientific literature, conference proceedings, etc. to find ideas that could be patented, so that we  
46 might find ourselves having to pay somebody else to use our own idea. Instead, we wanted the  
47 AirCore to be freely useable (and improved) by everyone, so that my patent (Tans, 2009) was  
48 intended to be a defensive action!

49 We realized that AirCore technology could become extremely useful for the validation of  
50 satellite retrievals of column-averaged mole fractions of greenhouse gases. The measurements of  
51 a gas sample captured by the AirCore are calibrated, but care has to be taken, as with all air  
52 samples in containers, that no artefacts are introduced by the container or by gas handling  
53 procedures. In contrast, remote sensing estimates of greenhouse gases can in principle never be  
54 calibrated. Metrology, the science of measurement, defines what a calibration is. Using a  
55 measurement standard, one presents the measurement method with a known value, under  
56 controlled conditions, so that the measurement indication is related to a quantity value  
57 (paraphrased from VIM3, JCGM 200:2008). In the case of greenhouse gases in the atmosphere  
58 the conditions cannot be controlled. In addition, we realized that the regular deployment of  
59 AirCores could be a cost effective way to monitor and study an evolving atmospheric circulation  
60 as climate change progresses, as proposed by Fred Moore-(Moore et al., 2014).

61 Developments of the AirCore by various groups has been described in other papers, for example  
62 by Wagenhäuser et al. (2021) and Membrive et al. (2017). However, there has not been a  
63 comprehensive treatment of fill dynamics, nor a detailed look at mixing. Hence this paper.

64

## 65 **2. The physical principle that makes the AirCore work – molecular diffusion**

66 Diffusive mixing over large distances is exceedingly slow, but there is another use of diffusion.  
67 Flow inside the tube is laminar, which has maximum speed in the center and zero speed at the  
68 wall. With velocities that differ from zero to some finite value, why does laminar flow **not**  
69 “smear out” our tape recorder signal by mixing air parcels that came in at different times? Again,  
70 molecular diffusion comes to the rescue. Using the square root relationship above, if the inner  
71 radius of the tube is 0.3 cm, it takes a CO<sub>2</sub> molecule on average only 0.03 s (at 1 bar pressure) to

72 diffuse from the wall to the radius where the velocity equals the average velocity inside the tube.  
73 Any molecule will be close to the wall, as well as near the center, of the tube many times per  
74 second. Therefore the speed of all molecules in the long direction of the tube, averaged over a  
75 few seconds, is very nearly the same. However, the AirCore idea does not work so well for  
76 liquids. In water the molecular diffusivity is ~10,000 times lower than in air at 1 bar, so that the  
77 smearing of a tape recorder signal could be very large. To compensate for such low diffusivity  
78 both the diameter of the tube and the flow speed will have to be kept low, and there will also be  
79 capillary effects. Water may be attracted to, or repelled by, the tube wall, influencing the flow.

80 The AirCore collects a continuous sample. Instead of valves, distance in the tube is used to keep  
81 separated the air that has been sampled from different pressure altitudes. The number of  
82 independent samples (the inverse of vertical resolution) in the tube decreases as the time between  
83 collection and measurement becomes longer. The measurement, or “read-out” of the vertical  
84 profile, is carried out by attaching an analytical instrument to one end of the tube and a cylinder  
85 with air of well-known composition to the other end. The latter pushes the sampled air slowly  
86 through the analyzer. The procedure, as well as various tests of mixing, has been described by  
87 Karion of GML (2010).

88

### 89 3. Dynamics of the fill process

90 How do we accurately associate position in the tube with the geometric altitude or pressure  
91 altitude that the sample at that position came from? It is the first question we address in this  
92 paper. The filling does not occur uniformly as a function of pressure altitude. The second  
93 question is how far the mixing of adjacent air parcels extends as a result of molecular diffusion,  
94 and secondarily as a result of the flow itself will be addressed in section 6. I wrote the first  
95 version of the fill dynamics calculation algorithm to make the association of altitude with  
96 position in 2005, called rocketfall.pro, coded in Interactive Data Language (IDL). Undergraduate  
97 students in the engineering department at the University of Colorado were getting ready to put an  
98 AirCore on a NASA rocket, and I was we were worried about there not being enough time to  
99 passively collect air from the stratosphere as the rocket was falling at supersonic speeds. There  
100 have been several successive versions of the algorithm since then. An intermediate version was  
101 translated from IDL, first into Matlab by Colm Sweeney of GML in 2013, and in 2017 from  
102 Matlab into Python by Jonathan Bent of GML. The significantly improved IDL version of July  
103 2021 is described in this paper here.

104 We use a fluid dynamics model and a subset of flight data, namely the time, pressure and  
105 temperature of outside air and the temperature of the tube as input data. The starting point is  
106 Poiseuille’s equation for steady state laminar flow in a tube with circular cross section:

$$107 \quad Q_m = \frac{-\rho \pi r^4}{8 \eta} \frac{dP}{dz}, \quad \text{or} \quad Q_n = \frac{-\rho_n \pi r^4}{8 \eta} \frac{dP}{dz} \quad \text{Eq. (1)}$$

108 in which  $Q_m$  is mass flow ( $\text{kg s}^{-1}$ ),  $Q_n = Q_m/M$  is amount flow ( $\text{mol s}^{-1}$ ) with  $M$  molecular weight  
 109 of dry air ( $0.02896 \text{ kg mol}^{-1}$ ),  $\rho$  is gas density ( $\text{kg m}^{-3}$ ),  $\rho_n$  is amount density ( $\rho/M$  in  $\text{mol m}^{-3}$ ),  $\eta$   
 110 is viscosity ( $\text{kg m}^{-1} \text{ s}^{-1}$ ),  $r$  is tube radius (m),  $P$  is pressure in Pascal ( $\text{kg m}^{-1} \text{ s}^{-2}$ ), and  $z$  is  
 111 distance along the tube (m). Pressure is given by the ideal gas law as  $P = (n/V) RT$ , with  $n/V = \rho_n$   
 112 the number density in  $\text{mol m}^{-3}$ ,  $T$  is temperature in degrees Kelvin (K), and  $R$  the universal gas  
 113 constant,  $8.3144 \text{ J mol}^{-1} \text{ K}^{-1}$ . The flow velocity is parabolic as a function of radius, zero at the  
 114 wall, and maximum in the center where the speed is twice the average speed.

115 The viscosity ( $\eta$ ) depends on temperature, but it is very nearly independent of pressure in our  
 116 range of interest. The latter is of primary importance to the fill process. A simple approximate  
 117 molecular expression for viscosity is  $\eta \cong (1/3) \rho \bar{c} \lambda$ , in which  $\bar{c}$  is the average molecular speed  
 118 and  $\lambda$  is the mean free path between collisions which is inversely proportional to  $\rho$  (Jeans, 1952)  
 119 so that it cancels the factor “ $\rho$ ” in  $(1/3) \rho \bar{c} \lambda$ . Since the volume flow ( $\text{m}^3 \text{ s}^{-1}$ ) is  $Q_v = Q_m/\rho$ , Eq.  
 120 (1) states that the volume flow depends on viscosity, but not on gas density. It takes the same  
 121 amount of force (pressure difference) to push a the same-volume flow irrespective of the density  
 122 of air in that volume. During steady flow through any tube the flow needs to speed up at the low  
 123 pressure end to conserve mass, so that the pressure gradient always steepens at the low pressure  
 124 end.

125 The  $z$ -coordinate is for position along the length of the tube. The pressure change at any point in  
 126 a small section of the tube with length  $dz$  can be due to temperature change or to more amount  
 127 flow coming in from  $z$  than leaving from  $z+dz$ . The latter term is

$$128 \quad \frac{d\rho_n}{dt} = - \frac{1}{\pi r^2} \frac{dQ_n}{dz}, \quad \text{so that}$$

$$129 \quad \frac{dP}{dt} = \rho_n R \frac{dT}{dt} + RT \frac{d\rho_n}{dt} = \frac{P}{T} \frac{dT}{dt} - \frac{RT}{\pi r^2} \frac{dQ_n}{dz} \quad \text{Eq. (2)}$$

130 Because if we assumed that the tube cross section is round (not elliptical for example) the  
 131 amount flow  $Q_n$  is given by Poiseuille’s equation, and Eq. (2) can be represented numerically in  
 132 a very efficient manner. In that case the flow is in effect solved as a succession of steady state  
 133 flows that evolve slowly in time and along the length of the tube. In the rest of this section we  
 134 will discuss a number of assumptions we are making for our “succession of steady state flows”  
 135 approximation to Eq. (2) to be satisfactory.

136 The first one is that inertial effects, i.e. accelerations, die out very rapidly. Suppose we suddenly  
 137 set the pressure gradient that is driving the flow to zero. What is the time scale for the flow to die  
 138 down? We can estimate the time it takes for the flow to adjust by using Eq. (1). The average  
 139 speed of the flow is  $\mathbf{v}_{\text{avg}} = Q_v/(\pi r^2) = (r^2/8\eta) (\Delta P/\Delta z)$ . The momentum of the flow in length  $\Delta z$  is  
 140  $\mathbf{v}_{\text{avg}} \rho \pi r^2 \Delta z$  which equals  $Q_m \Delta z$  (neglecting the sign). The rate of change of momentum is  
 141 given by the frictional force which is equal and opposite to the pressure force that was driving

142 the flow in Eq. (1). The adjustment time scale of the flow is momentum divided by the frictional  
 143 force,

$$144 \quad \tau = \frac{Q_m \Delta z}{\Delta P \pi r^2} = \frac{\rho r^2}{8 \eta} \quad \text{Eq. (3)}$$

145 For a tube with a radius of 3 mm and  $\rho$  corresponding to 1 bar and 285 K,  $\tau \cong 0.07$  s. At an  
 146 altitude where the density is 10 times lower ( $\sim 18$  km),  $\tau \cong 0.007$  s. Recently NOAA GML has  
 147 been flying AirCores with  $r \cong 1.46$  mm, for which the adjustment time at 1 bar and 285 K is  $\tau \cong$   
 148 0.017 s. A succession of steady state flows is indeed a very close approximation.

149 Next we assume that the temperature of the gas is the same as that of the wall. How rapidly does  
 150 the temperature of the gas equilibrate with the wall of the tube? The heat capacity of a volume of  
 151 air is  $c_p \rho_n \cong (7/2) R * P/RT$  in which  $c_p$  is the molar heat capacity at constant pressure and  $\rho_n$  is  
 152 the number density ( $\text{mol m}^{-3}$ ) of the gas, so that  $c_p \rho_n$  has units of  $\text{J m}^{-3} \text{K}^{-1}$ . The heat  
 153 conductivity of gas is  $\kappa \cong (1/3) c_v \rho_n \mathbf{c} \lambda$  (Jeans, 1952) in which  $c_v$  is the molar heat capacity at  
 154 constant volume,  $\mathbf{c}$  is the average speed of individual molecules and  $\lambda$  the mean free path. It has  
 155 units of  $(\text{J/s}) \text{m}^{-2} (\text{K/m})^{-1}$ , the heat flow per area per temperature gradient. As in the previous  
 156 paragraph we divide the heat energy change corresponding to  $\Delta T$  in a volume of gas residing in a  
 157 length  $\Delta z$  by the heat flow from the wall assuming the temperature gradient is close to  
 158  $(\Delta T/(0.5r))$ . That gives

$$159 \quad \tau = \frac{c_p \rho_n \pi r^2 \Delta z \Delta T}{(1/3) c_v \rho_n \mathbf{c} \lambda 2\pi r \Delta z \Delta T / (0.5r)} = \frac{c_p}{c_v} \frac{3 r^2}{4 \mathbf{c} \lambda} \quad \text{Eq. (4)}$$

160 which has units of seconds. For  $r = 3$  mm and  $\lambda$  corresponding to 1 bar, and 285 K, the  
 161 adjustment time is  $\tau \cong 0.31$  s, and shorter at lower pressures. For  $r = 1.46$  mm  $\tau \cong 0.07$  s.

162 Is the flow always laminar as Eq. 1 assumes? If Reynolds number,  $Re = (\rho v_{avg} d)/\eta$ , in which  $d$  is  
 163 the diameter of the tube, stays below 1000, the flow will remain laminar.  $Re$  is estimated from  
 164 the calculated velocities,  $\rho/\eta$ , and tube dimensions for every flight. It is highest just before  
 165 landing when it typically has a value of  $\sim 15$ .

166 The tube is wound up in a coil with typical diameter 20 to 30 cm. As the flow goes around the  
 167 coil there will be a centrifugal force away from the center of the coil. The centrifugal force is  
 168 greatest where the flow has the maximum velocity,  $2 v_{avg}$ , very near the center of the tube. This  
 169 sets up a secondary flow in the plane perpendicular to the main flow, outward in the center of the  
 170 tube and back along the walls. The location of maximum velocity is also pushed outward a bit.  
 171 This increases flow resistance leading to slightly lower  $Q_m$  for the same pressure gradient in the  
 172 dimension  $z$  along the length of the tube. However, there are other subtle effects with the  
 173 opposite sign that could facilitate the flow a little (Berg, 2005). Correction factors to flow in a  
 174 straight tube have been calculated using Dean's number,  $De = Re (r/R)^{0.5}$ , in which  $Re$  is  
 175 Reynolds number and  $R$  is the coil radius. NOAA GML has flown AirCores with  $r/R$  from 1/50

176 to 1/70. Thus  $De$  is always smaller than  $15 (0.02)^{0.5} \cong 2$  during a flight. Berg et al. (2005)  
177 present data to estimate that the relative flow correction is smaller than  $+1 \cdot 10^{-5}$  for our  
178 parameters. If we were to wind our coil much tighter, say with  $r/R$  of 1/20, then the maximum  
179 relative flow correction during a flight would be  $+2 \cdot 10^{-4}$  for the same Reynolds number.  
180 Therefore we can neglect the corrections for the tube coil curvature.

181 If the tube is elliptical (as a result of bending, for example) instead of circular, we can use there  
182 is a good approximation for the change in flow resistance. Following Lekner (2019), Eq.1 can be  
183 written for volume flow as  $(\eta Q_v) / (dP/dz) = \pi r^4 / 8$ , neglecting the sign. Note that  $\pi r^4 / 8$   
184 equals  $A^3 / (2 P^2)$  for a circular cross section, with  $A$  the cross sectional area, and  $P$  the perimeter  
185 of the tube. Lekner shows that  $A^3 / (2 P^2)$  applies quite generally for many cross sectional shapes.  
186 So if the tube is somewhat squashed into an ellipse with major axis 1.05 times the original  
187 radius, and a minor axis slightly smaller (in order to keep the perimeter the same) than 0.95 times  
188 radius, the term  $A^3 / (2 P^2)$  has become  $\sim 1\%$  smaller. This correction is not a-major, but easy to  
189 apply if needed-effect.

190 We assumed the ideal gas law. Non-ideality is often described by the virial expansion relating  
191 pressure and density,  $PV/nRT = 1 + B(n/V) + C(n/V)^2 + \dots$ . Note that  $n/V$  is called  $\rho_n$  above.  
192 Taking only the second (and largest) virial coefficient  $B$  ( $m^3/mol$ ) into account we can  
193 approximate the number density  $\rho_n$  as  $(P/RT)(1-BP/RT)$ . The relative change of number density  
194 is thus  $BP/RT$  which has dimension one. At 300 K and 1 bar,  $B$  is  $-7.3 \cdot 10^{-6} m^3/mol$   
195 (Sevast'yanov, 1986) which leads to a relative density increase of  $2.9 \cdot 10^{-4}$ .  $B$  increases to  $-18.9$   
196  $\cdot 10^{-6}$  and  $-37.8 \cdot 10^{-6} m^3/mol$  at 250 K and 200 K respectively, but at the higher altitudes the  
197 density is lower so that the largest non-ideality effect occurs near the ground. Therefore the  
198 fractional density increase relative to ideal gas during a flight remains well below 0.001

199 When the mean free path increases at lower pressures there could be “wall-slip”, non-zero  
200 velocity at the wall which can be modeled as an effective decrease in viscosity increasing the  
201 volume flow. Berg (2005) gives an approximate expression for the factor by which the flow  
202 increases,  $1 + 4 K_{slip} Kn$ , where  $K_{slip}$  is a number close to 1 which depends on intermolecular  
203 forces, and  $Kn$  is the Knudsen number,  $\lambda/d$ , with  $d$  being the internal diameter of the tube. At  
204 high altitude, say  $10 \text{ hPa-millibar (mb)}$ ,  $\lambda \sim 7 \cdot 10^{-4} \text{ cm}$ , so that  $Kn \sim 0.001$  for  $d = 0.6 \text{ cm}$ . For  $d =$   
205  $0.3 \text{ cm}$  the flow would be increased by a factor 1.009 at  $10 \text{ hPa mb}$ .

206 When  $Kn$  becomes larger than  $\sim 0.01$  a transition region of pressure is entered in which the flow  
207 changes gradually from bulk flow of gases, laminar in our case, to molecular flow (O’Hanlon,  
208 1980). In the latter flow regime the gas sample enters the tube as individual molecules, and gases  
209 with higher molecular speed (lower mass) enter the tube more rapidly, so that the air sample may  
210 not represent the composition of outside air, whereas in bulk flow an overwhelming fraction of  
211 all molecules are equally swept along. As an example, for an AirCore with opening diameter of  
212  $0.3 \text{ cm}$  this flow transition starts at a pressure altitude of  $\sim 2 \text{ hPa mb}$ . Therefore, approximately 43  
213 km might be the highest altitude that can be sampled with this diameter opening without first

214 quantitatively investigating molecular flow effects, although this limit depends also on the  
215 sampling accuracy we require.

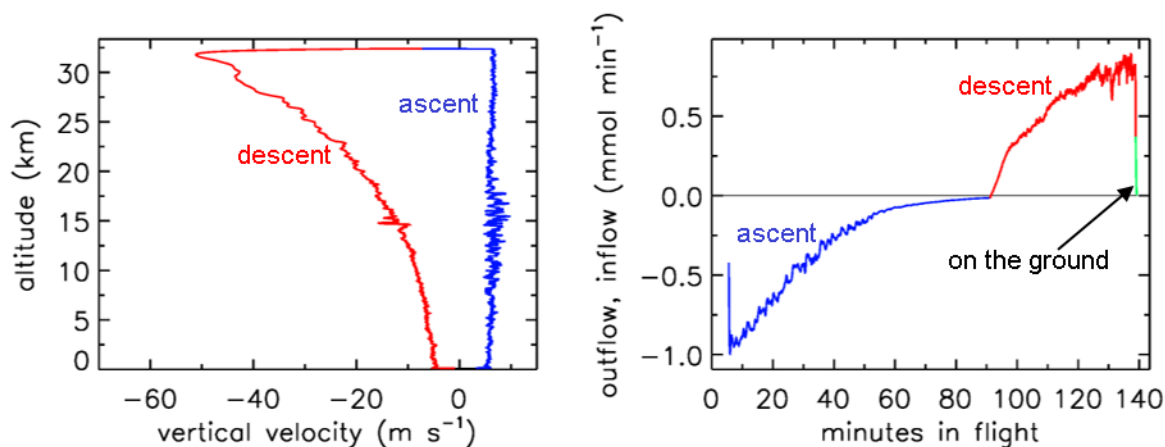
216 The above expressions for viscosity,  $\eta \cong (1/3) \rho \mathbf{c} \lambda$ , and heat conductivity,  $\kappa \cong (1/3) c_v \rho_n \mathbf{c} \lambda$ ,  
217 and similar for diffusivity,  $D \cong (1/3) \mathbf{c} \lambda$  are approximate. More precise forms of these equations  
218 vary depending on the treatment of intermolecular forces. Instead, we use a curve fit to empirical  
219 data for viscosity in dry air as a function of temperature, as presented by Kadoya (1985). The  
220 empirical data show, as expected, that there is no dependence on pressure in our range of  
221 interest.

222 For diffusivity of trace gases in air as a function of temperature and pressure we use the  
223 empirical equation presented by Massman (1999),  $D(T,P) = D_0 (P_0/P) (T/T_0)^{1.81}$ .  $D_0$  is the  
224 diffusivity, different for each trace gas in air, at 1 atmosphere air pressure ( $P_0$ ) and 0 degrees  
225 centigrade ( $T_0$ ). This will be used when we calculate mixing of air samples entering the AirCore  
226 sequentially. Mixing is caused both by molecular diffusion ( $X_{rms} = (2Dt)^{0.5}$ , see above) and by  
227 the quadratic velocity profile of laminar flow, with zero speed at the wall and maximum speed in  
228 the center. The latter is called Taylor diffusion (Karion, 2010), and is given by a diffusivity  
229 constant  $D_T = \mathbf{v}_{avg}^2 r^2 / (48 D)$  which has the same dimensions as  $D$ ,  $m^2 s^{-1}$ .

230

#### 231 4. Calculated in- and outflow results for some flights

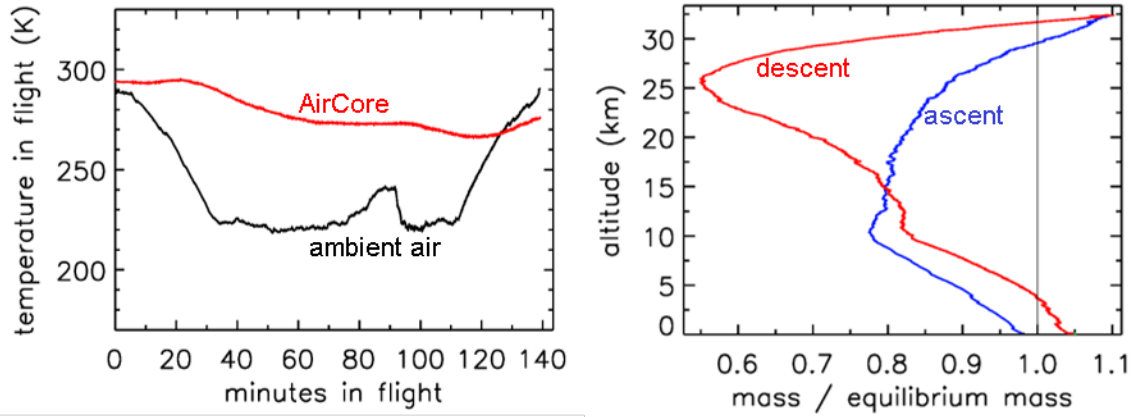
232 In Figures 1– 4 the flight is shown of a small diameter (1/8 inch, internal diameter 2.92 mm)  
233 AirCore (GMD008), with 93 m length and internal volume 619 cc, near Trainou, France (48.0  
234 °N, 2.1 °E) on 20 June 2019. The ascent velocity of the helium balloon is nearly constant, while  
235 the rate of mass outflow decreases steadily as a function of time as the pressure outside and  
236 inside the AirCore drops. The descent velocity with parachute accelerates nearly linearly in the



237

238 *Figure 1. Descent velocity (negative) and rate of fill air outflow followed by air sample inflow*  
239 *during flight of GMD008. Blue, ascent; red, descent; green, on the ground*

240 first 10 seconds to about  $50 \text{ m s}^{-1}$  as the air density pressure at high altitudes is too low for air  
 241 friction to slow it down enough. The initial descent can be a chaotic tumble until the parachute  
 242 gets a “grip”. Outflow and inflow in the tube are calculated with the fill dynamics program  
 243 described below in section 8.



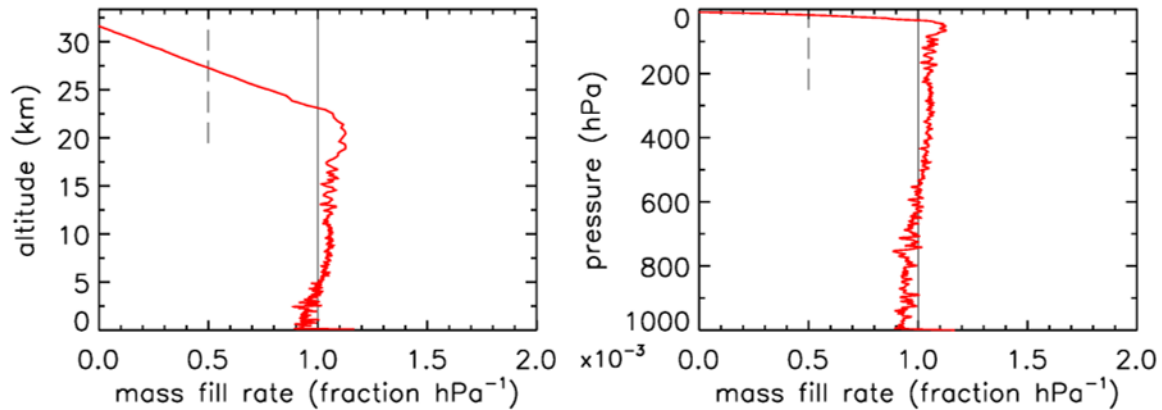
244  
 245 *Figure 2. Flight of GMD008. Left panel: Temperatures in degrees Kelvin. AirCore tube, red;*  
 246 *outside air, black. Right panel: How far the mass inside the tube is out of equilibrium with*  
 247 *ambient air. Blue, ascent; red, descent.*

248 In Figure 2 the outside air temperature first cools while in the troposphere, then becomes nearly  
 249 constant in the tropopause, and starts increasing again higher into the stratosphere. GMD008 was  
 250 well insulated but still partially followed the outside temperatures with a delay. In the right panel  
 251 the total amount of air in the tube is plotted relative to how much it would be if it had the same  
 252 pressure and temperature everywhere in the tube as the outside air. Vertical line: the ratio equals  
 253 1 if they were the same. During ascent in the troposphere (up to about 10 km) the air in the tube  
 254 is warmer, and thus less dense, than outside air. In the tropopause the tube continues to cool so  
 255 that the “deficit” becomes smaller, but at higher altitudes, around ~25 km the amount by which  
 256 the pressure in the tube is higher than outside becomes substantial relative to the low outside  
 257 pressure – as a result the ratio at ~34 km altitude becomes a bit larger than 1. Then, during  
 258 descent the outside pressure increases rapidly and the inflow cannot keep up because the  
 259 viscosity of air at low pressure is the same as at 1 bar (see section 3). Back in the troposphere the  
 260 tube warms up, but much more slowly than outside air. When the tube hits the ground, it is  
 261 colder than ambient air temperature so that the ratio is greater than 1.

262 In Figure 3 the fill rate is plotted (mol per hPa of ambient pressure gain) divided by the final fill  
 263 (moles of air) at valve closure. At sea level the final pressure is close to 1013 hPa, so that the  
 264 average fraction of final fill amount per hPa will be approximately 0.001. The uptick upon

265

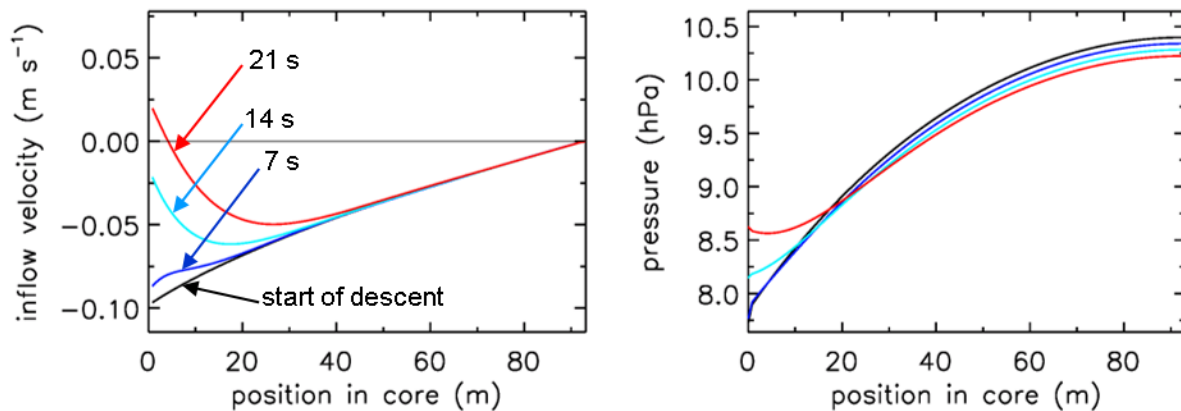




266

267 *Figure 3. Flight of GMD008. The vertical line at  $1.0 \cdot 10^{-3}$  is approximately the expected rate of*  
 268 *sample inflow. The dashed line at  $0.5 \cdot 10^{-3}$  represents the half-fillrate point (see main text).*

269 landing (very close to the x-axis) is the result of a bit of air still entering the tube initially while  
 270 ambient pressure stops changing, neglecting high frequency noise. If the valve is not closed  
 271 quickly this will reverse because as the tube warms up on the ground, the last air that came in  
 272 will be expelled. At high altitudes it takes time for the fill to start because ambient pressure  
 273 needs to build up enough to force the air in. The highest altitude was 32.4 km, at 7.7 hPa ambient  
 274 pressure. The fill starts at 31.6 km and pressure 8.5 hPa, slowly at first, and gradually becomes  
 275 faster. To compare the start of fill between AirCore designs with different diameters and valves,  
 276 we could take the point at which the fill rate is  $0.5 \cdot 10^{-3}$ . In this case the “half-fillrate point” is at  
 277 27.3 km and ambient pressure of 17.3 hPa. We will see below that the fill starts much faster with



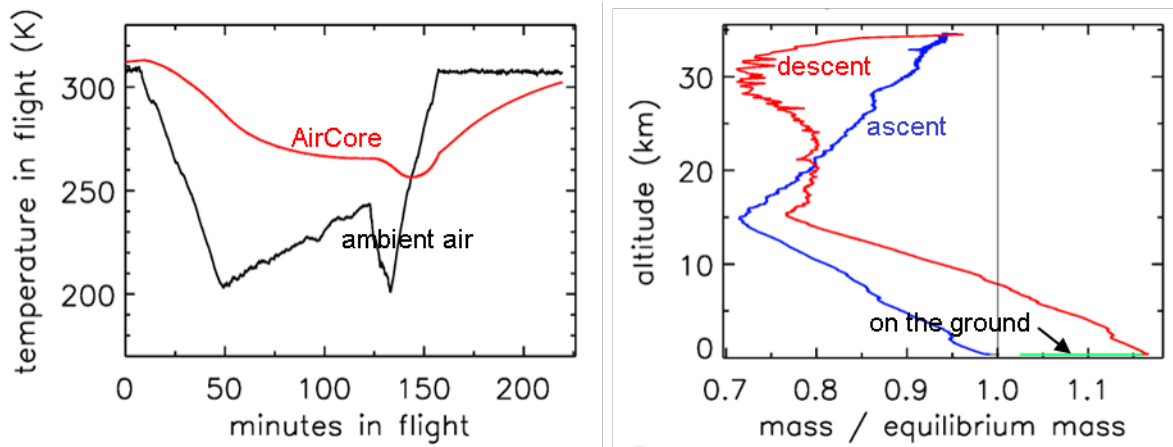
278

279 *Figure 4. Flight of GMD008. The turnaround at high altitude. Inflow velocity and pressure*  
 280 *inside the AirCore from the moment the ascent stops and descent begins. Times are in seconds*  
 281 *after start descent. Black, 0 seconds after start of descent; dark blue, 7 s after start; light blue,*  
 282 *14 s; red, 21 s.*

283 larger diameters. Figure 4 shows detail of flow and pressure inside the tube for the flight on 20  
 284 June 2019 at the start of descent. Initially the inflow velocity is negative. It is outflow, zero at the

285 closed end and increasing toward the open end. ~~The velocity has to jump up inside the flow~~  
 286 ~~restrictions of the valves and possibly the dryer at the entrance of the AirCore, adjacent to~~  
 287 ~~position at 0 m.~~ After 14 seconds into the descent (light blue curve) the outflow has weakened  
 288 considerably and the pressure gradient near the open end is much smaller. Inflow starts after 19  
 289 s, very slowly at first, while at the same time the flow in most of the tube is still negative  
 290 (outflow toward the open end), consistent with the pressure gradients.

291 Let us look now at an AirCore with larger diameters (Figure 5). This one had 26 m of 1/4 inch  
 292 (internal diameter 5.84 mm ~~internal diameter~~) tubing at the open end and 37.6 m of 1/8 inch  
 293 (2.67 mm internal diameter) tubing at the closed end, with a total internal volume of 9890 cc.  
 294 The high-altitude fill history of the two AirCores is summarized in Table 1. In front of the open  
 295 end was a valve, the dryer (large magnesium perchlorate particles), and then another valve  
 296 connecting to the AirCore tube. It was flown in Oklahoma, U.S. (37.2 N, 97.8 W), on 23 July  
 297 2013. While the

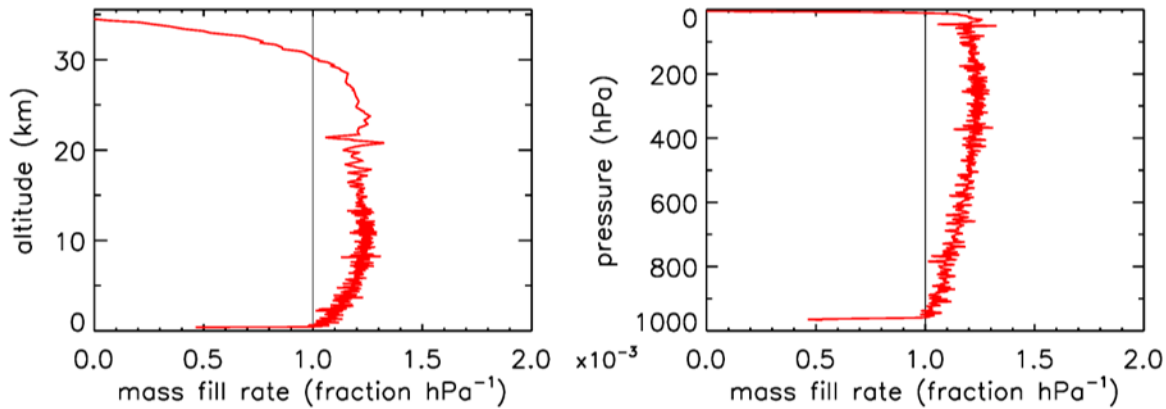


298

299 *Figure 5. Flight of AC01 in Oklahoma.*

300 AirCore used near Trainou, France, experienced a temperature range 15 K, the less well  
 301 insulated AC01 in Oklahoma saw a range of 57 K. At the moment of landing the average  
 302 temperature of the tube was ~40 K cooler than ambient. Fig. 5 shows the flight data until the  
 303 moment of valve closure. The valve remained open for 62 minutes after landing, so that the  
 304 lowest portion of the atmospheric sample, between pressure altitudes of 844 and 967  $hP_{amb}$   
 305 (1565 to 352 m), was expelled as the AirCore warmed up. The descent started at 34.6 km altitude  
 306 (4.6  $hP_{amb}$ ). The lowest relative mass deficit (~27%) was reached around 30 km, in contrast to

307 the Trainou flight with 50% at 27 km altitude respectively. The half-fillrate point of

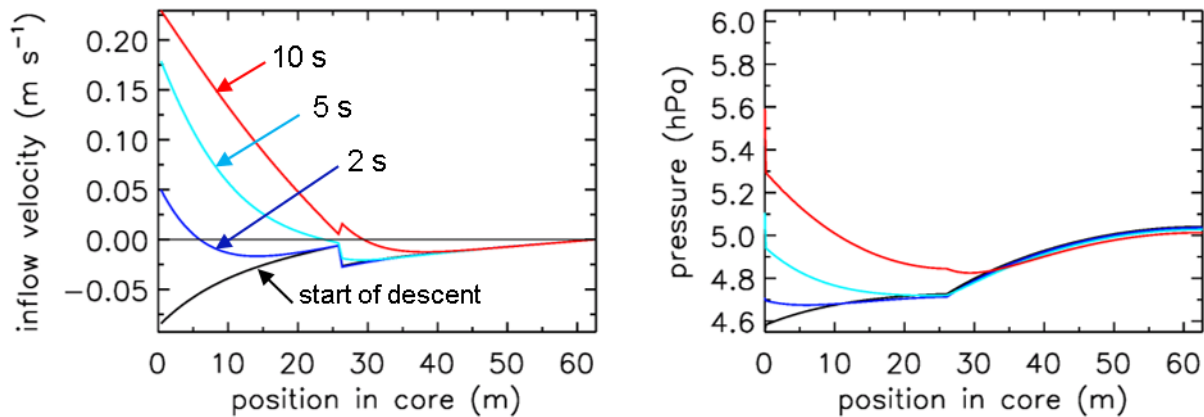


308

309 *Figure 6. Flight of AC01 in Oklahoma. Compare with Figure 3.*

310  $0.5 \cdot 10^{-3}$  per hPa is reached at 33.2 km altitude and 6.2 hPa of ambient pressure, a sampling  
 311 altitude gain of almost 6 km compared to the Trainou flight. If the total amount of initial fill air  
 312 that remained in the tube can be carefully measured that would give an independent estimate  
 313 of the pressure altitude where the fill (slowly) started. determination of the half fillrate point  
 314 estimated here. The fill rate below ~8 km falls off noticeably as the warming rate of the tube  
 315 speeds up. The negative mass fill rate while on the ground cannot be portrayed in Fig. 6 because  
 316 ambient pressure remains constant. This AirCore design contains a larger fraction of  
 317 stratospheric air than GML008, mostly because of the wider diameter, but also because it was  
 318 allowed to cool more.

319



320

321 *Figure 7. Flight of AC01 in Oklahoma, showing inflow velocity and pressure gradients.*  
 322 *Compare with Figure 4. Black, 0 seconds after start of descent; dark blue, 2 s after start; light*  
 323 *blue, 5 s; red, 10 s. Note the much smaller fill delay than in Fig. 4. The pressure drop across*  
 324 *flow velocity inside the two valves and dryer is visible has not been plotted here, but the pressure*  
 325 *drop across them has.*

326 If one wants to sample still higher into the stratosphere the diameter of the first 10 to 20 m at the  
 327 open end needs to be widened further than 6 mm diameter (Table 1). All of this is consistent with

328 Table 1. Comparison of start of fill process for two AirCore configurations

AirCore Trainou 2019	Int. Dia (mm)	Length (m)		Aircore Oklahoma 2013	Int. Dia (mm)	Length (m)
Aircore tubing	2.16	0.76		AirCore tubing	5.84	25.9
AirCore tubing	2.92	91.5		AirCore tubing	2.67	36.6
AirCore tubing	2.16	0.76				
internal volume		619 cc		internal volume		890 cc
Fill history	Time (s)	Altitude (hPa),(km)		Fill history	Time (s)	Altitude (hPa), (km)
start descent	0	7.7, 32.4		start descent	0	4.6, 34.6
start fill	19	8.5, 31.6		start fill	2	4.7, 34.4
half fillrate	123	17.4, 27.3		half fillrate	7	6.3, 33.2
full fillrate	266	34.2, 23.1		full fillrate	58	10.4, 30.2

329

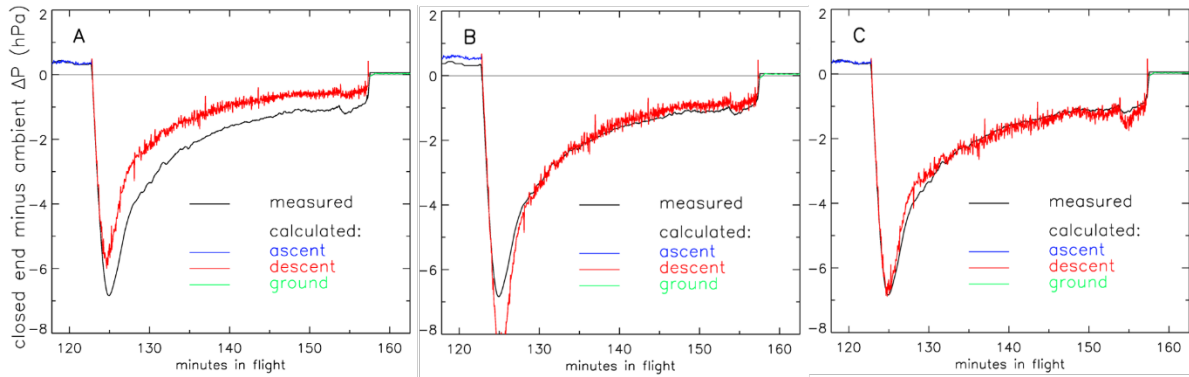
330 Fig. (7), where we also see that at the start of the descent the outflow velocity inside the tube  
 331 drops by a factor of  $\sim 4$  when, moving from the back to the open end, at 25.96 m the tube  
 332 diameter becomes wider by a factor of  $\sim 2$ . This applies of course also to the inflow as shown by  
 333 the red curve. At the same point the pressure gradient becomes less steep by the same factor of 4.  
 334 The fill starts at ambient pressure of 4.7-hPamb. We also note that in this case the pressure drop  
 335 inside the two valves and the dryer is a large part of the overall pressure drop across the entire  
 336 tube, an effect that becomes more pronounced as especially when the tube diameter gets is  
 337 larger.

338 In these calculations Iwe have experimented with another strategy to fill the AirCore. One could  
 339 launch it with both valves open, but the one in the back is closed as soon as the descent starts.  
 340 That would decrease the amount of fill air that remains in the back. However, the difference from  
 341 having the back valve closed during the entire flight is negligible-minuscule.

342

### 343 5. Valves

344 So far the treatment of valves and the dryer has been missing from this description. As a first  
 345 approximation we could treat the valves as short pieces of tubing with reasonably “average”  
 346 internal diameter and length such that their internal volume is correct. This does not provide  
 347 enough flow resistance, when we compare it to differential pressure measurements made during  
 348 some-flights between the closed end of the AirCore and the outside ambient air (Fig. ure 8).



349

350 *Figure 8. Pressure difference ( $\Delta P$ ) between closed end of tube and outside air during the*  
 351 *descent portion of flight of AC01 in Oklahoma as a function of elapsed time in flight. Black:*  
 352 *measured pressure difference (~~mb~~, ~~or~~ hPa). Red: calculated  $\Delta P$  with three different treatments of*  
 353 *the valves. A, fixed internal diameter and length; B, same as in A, but optimized; C, using*  
 354 *optimized  $C_v$  and  $X_{TPR}$  (see [main text](#)) values.*

355 In panel A we calculate that during the descent the air enters the tube too easily, so that the  
 356 altitudes assigned to the air sample in the stratosphere would be biased high. We could decrease  
 357 the chosen internal average diameter (~~not a well-defined value~~) of the valves (panel B),  
 358 optimized so that the difference between calculated and measured  $\Delta P$  during the entire descent,  
 359 from minute 123 to 157, is minimized. However, it is clear that this effective or apparent internal  
 360 diameter needs to change during the flight. Using  $C_v$  values and a description of choked flow is  
 361 clearly better. In panel C we have chosen the  $C_v$  and  $X_{TPR}$  ([see below](#)) values such that the  
 362 average difference from minute 123 to 157 is zero and the standard deviation of differences is  
 363 minimized. This implicitly includes any effects caused by the dryer in between the two valves.

364 The flow inside a valve can be complicated, with sharp corners, turbulence, sudden acceleration  
 365 through a flow restriction with its associated heating and cooling of the gas, etc. The industry has  
 366 introduced flow coefficients ( $C_v$  in the U.S., and  $K_v$  elsewhere) as an empirical approach to flow  
 367 calculations, as in the Swagelok brochure (2020). The expressions for air, slightly generalized  
 368 from Swagelok, for gas flow are as follows. For low pressure drop flow, we have

369

370 
$$Q_n = 6950 C_v \sqrt{P_1 \left(1 - \frac{X}{3 X_{TPR}}\right) \sqrt{\frac{X}{T_1}}} \quad (\text{Eq. 5a}),$$
 where  $Q_n$  is in liters per minute at standard

371 conditions of 1 bar and 0°C,  $P_1$  and  $T_1$  are pressure (bar) and temperature (Kelvin) upstream of  
 372 the valve,  $\Delta P$  is the pressure drop across the valve,  $X$  is the pressure drop ratio  $\Delta P/P_1$ , and  $X_{TPR}$   
 373 is the terminal pressure drop ratio between (0 and 1) above which we have choked flow. Under  
 374 choked flow conditions the flow is fully independent of  $P$  and  $T$  downstream of the valve. It is  
 375 also important to know that the flow coefficient  $C_v G_v$  is not a pure number, but has physical  
 376 quantities and units embedded in it.

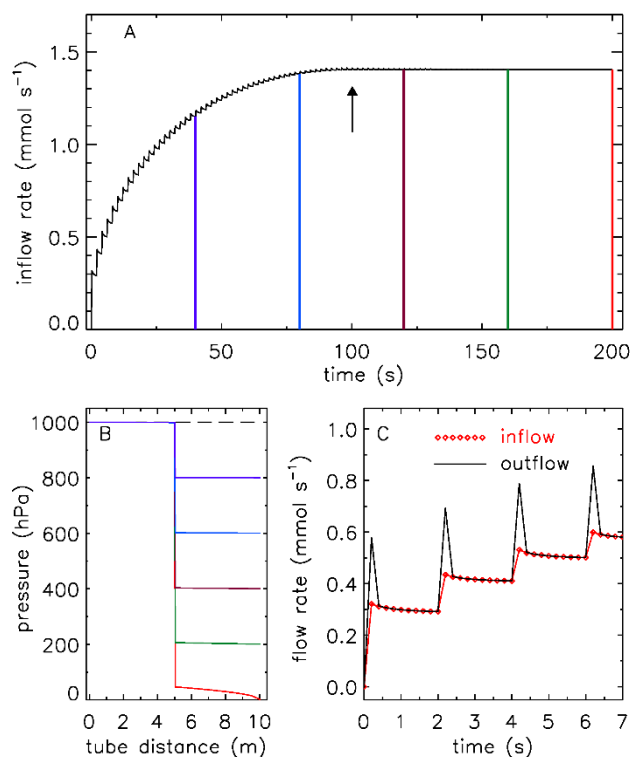
377 For a high pressure drop ( $X > X_{\text{TPR}}$ ), we have

378 
$$Q_n = 6950 C_v \sqrt{P_1} \frac{2}{3} \sqrt{\frac{X_{\text{TPR}}}{T_1}} \quad (\text{Eq. 5b}),$$
 which is obtained from the previous expression by

379 substituting  $X_{\text{TPR}}$  (a constant) for  $X$ . In these expressions we prefer to express the flow, instead  
380 of in standard L/min as in the Swagelok brochure, as 0.04403 mol/min. This is the same, when  
381 using the molecular weight of dry air (28.97 g/mol), as a mass flow of 1.276 g/min.

382 In Fig. 8C we optimized both  $C_v$  and  $X_{\text{TPR}}$  to get the best match for the calculated pressure  
383 difference across the AirCore with the observed history during the descent. The value of  $X_{\text{TPR}}$   
384 depends on valve design, and may not be the same when flow goes in the opposite direction.  
385 Many valves have an arrow for flow direction printed on them. For manyest AirCore flights  
386 differential pressure measurements have not been recorded. However, But the valves (and also  
387 dryers) could be tested with a standard procedure (see Fig. ure 9 as one example). Alternatively,  
388 or as a complementary check, a micro-spiking method during filling could be used  
389 (Wagenhäuser, 2021).

390 Figure 9 shows a potential test procedure for determining  $C_v$  and  $X_{\text{TPR}}$  values. The figure is  
391 drawn using the two expressions for  $Q_n$  above, for low flow and choked flow. Starting from a  
392 uniform pressure of 1 bar, the pressure at the downstream side is lowered in 10 hPamb-steps, at 2  
393 s intervals. In this example  $C_v = 0.01$  and  $X_{\text{TPR}} = 0.5$ , so that the transition to choked flow  
394 occurs at a pressure drop of 0.5 bar (panel A, upward arrow at 100 s). When the pressure at 10 m  
395 approaches zero, the flow speed is high, causing a significant pressure drop between 5 and 10 m.



396

397 *Figure 9. A potential test procedure to determine  $C_v$  and  $X_{TPR}$  values for valves. In this example*  
 398 *there is 5 m of 1/4" tubing (ID 5.84 mm) on each side. Outflow at the 10 m point (black curve) is*  
 399 *shown in panels A and C. There is a flow pulse at every step because the downstream 5 m*  
 400 *section empties quickly. The time resolution is 0.2 s. Inflow at 0 m is shown as red diamond*  
 401 *symbols in panel C. Panel B, pressure in the tube from time 0 (dashed line) at 40 s intervals,*  
 402 *corresponding to the colors in panel A.*

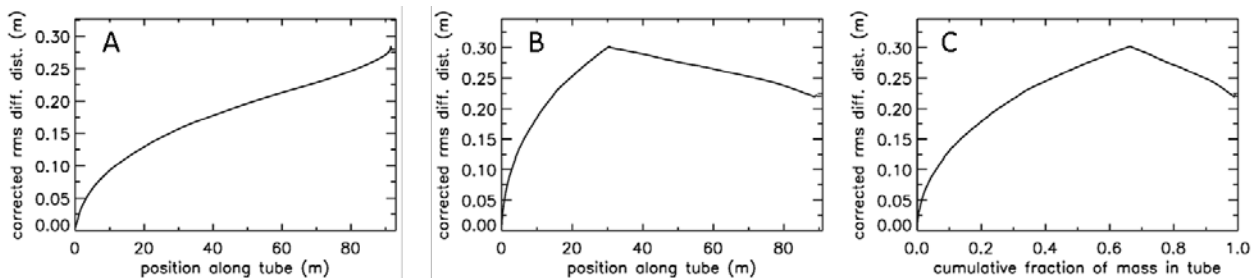
403

## 404 6. Mixing inside the tube

405 The fill dynamics calculation has produced time series of air density, pressure and temperature,  
 406 and flow velocity everywhere in the tube as a function of time, from the start of the fill process,  
 407 which begins a varying amount of time after the AirCore has started its descent, to the time of  
 408 valve closure. We divide the final amount of air in the tube at closure into 400-500 equal mass  
 409 packets. Starting from 400 we increase the number, which shrinks the size of each packet, until  
 410 the remaining fill air in the back of the tube comprises an exact integer number of packets. For  
 411 each mass packet, after it has entered the tube we follow it through the tube, as it is pushed  
 412 toward the back while being compressed by packets entering later. The time steps are defined by  
 413 when a new packet has fully entered, and they are longer at the start of the fill. The molecular  
 414 diffusivity  $D$  and the Taylor diffusivity  $D_T$  are different at each step. However, the amount of  
 415 spreading of a packet calculated at each time step “k” is decreased as the increasing pressure  
 416 compresses the packet further. So the contribution of each step to the final spreading at valve  
 417 closure is calculated by dividing the density during that time step by the final density in the tube.  
 418 We are thus accumulating the “ $2Dt$ ” term of  $X_{rms} = (2Dt)^{0.5}$ , with Taylor diffusion added:

$$419 \quad X_{rms} = \sqrt{2 \sum_k (D_k + D_{T,k}) \frac{\rho_k}{\rho_{final}} t_k} \quad \text{Eq. 6}$$

420 For an AirCore with (almost) uniform diameter we get mixing as in Fig. 10 A. Close to the open  
 421 end at position 0 m, there is very little mixing because the time to mix was short. Near the closed  
 422 end at 93 m the spread of mixing deviates from what see in the first approximately 2/3 of the  
 423 tube because the fill started slowly, giving extra mixing time for the high altitude samples that  
 424 were later pushed to the back.



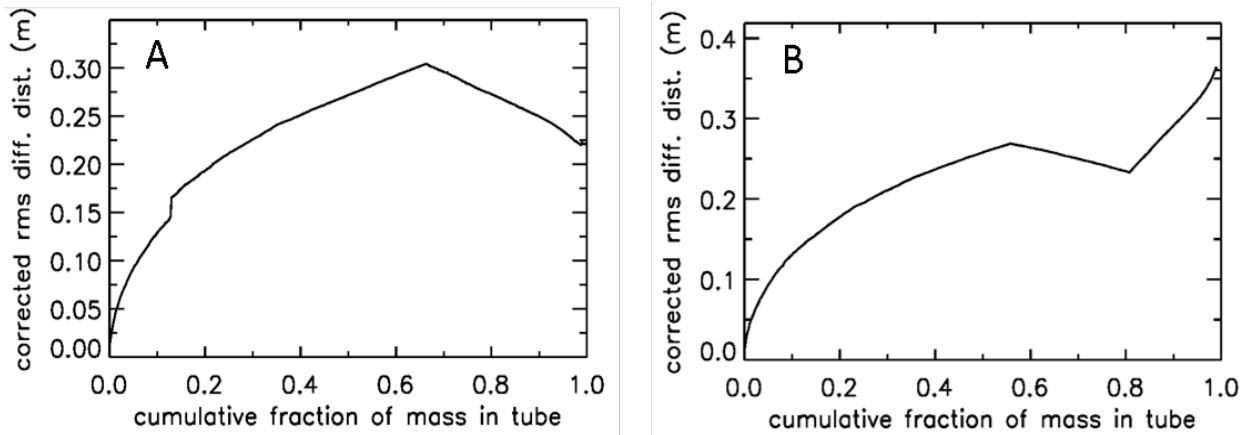
425

426 *Figure 10. Root-mean-square diffusive mixing when the valve at position 0 is closed. Panel A,*  
 427 *Flight of GMD008 in Trainou. Panel B, the same flight data, but used to calculate the filling of a*  
 428 *different AirCore, with 30.9 m of 1/4" tubing at the open end, and 60.1 m of 1/8" at the closed*  
 429 *end. Panel C, same as B, but plotted as cumulative fraction of total mass, from 0 to 1.*

430 For an AirCore with two sections of different diameter we see an interesting effect (Fig.10 B).  
 431 The air that comes in at high altitudes and ends up in the back of the tube, has to go through  
 432 the 1/4" section first. When a packet enters the 1/8" section, its spread becomes approximately  
 433 four times larger, while its 2Dt accumulation term stays the same. Approximately, because the  
 434 inner diameters (ID) matters, not the outer (OD). To correct for the jump we add another factor  
 435 to Eq. 6, and we will call this corrected rms diffusion distance:

$$436 \quad X_{\text{rms}} = \sqrt{2 \sum_k (D_k + D_{T,k}) \frac{\rho_k}{\rho_{\text{final}}} \frac{(d\text{vol}/dx)_k}{(d\text{vol}/dx)_{\text{ref}}} t_k} \quad \text{Eq. 7}$$

437 In Eq. 7 dvol/dx is the increment in volume per increment in length of the tube, while  $(d\text{vol}/dx)_{\text{ref}}$   
 438 is the total volume divided by the total length, both in units of  $\text{m}^2$ . This prevents a jump at the 30  
 439 m position, but more importantly, what matters for mixing is the spread relative to total mass in  
 440 the tube, not whether it is in the 1/4 or 1/8" section. From now on we call this configuration "1/4  
 441 -1/8". Fig. 10 B shows that air closer to the back has been in the 1/4" section for a shorter time,  
 442 and thus experienced less mixing relative to mass. When plotting mixing not as a function of  
 443 position, but as a function of cumulative mass in the tube, Fig. 10 C also shows that the 1/8"  
 444 section contains approximately 1/3 of the total air sample.



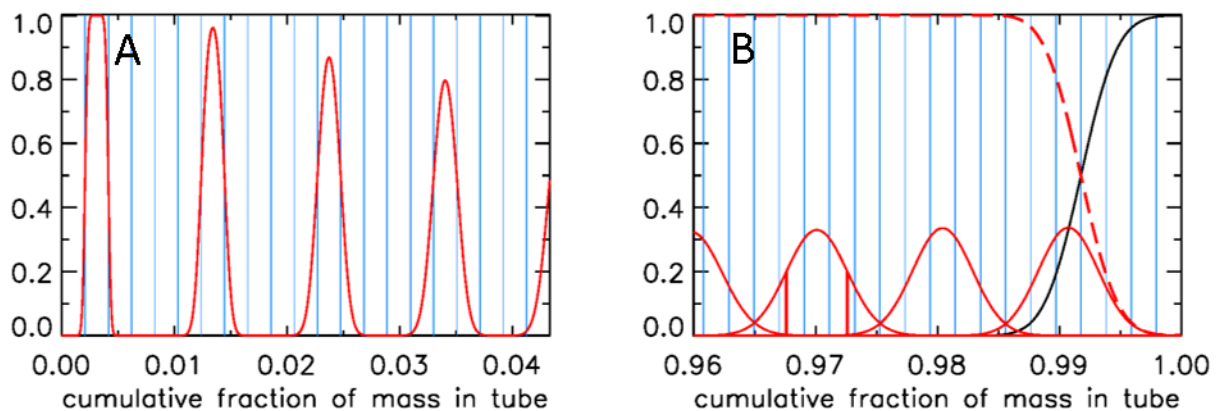
445  
 446 *Figure 11. Two additional cases of mixing upon valve closure. Panel A, same AirCore 1/4 -1/8,*  
 447 *but the flight data have been changed. Panel B, same flight data as in Fig. 10A, but the AirCore*  
 448 *configuration is 1/4 - 1/8 - 1/4.*

449 In Fig. 11A when the tube had descended to 850 mb, the atmospheric pressure data were  
 450 changed to simulate an updraft (lowering outside pressure) followed by a downdraft. The most  
 451 recent 7 mass packets were lost from the tube during the updraft, and replaced by new air during  
 452 the downdraft (above average rate of increase of outside pressure). As a result, the air sample



453 that just escaped from being lost is now adjacent to the replacement air, creating the jump in rms  
 454 mixing because it has been  $\sim 15$  s longer in the tube than the first replacement air entering. In Fig.  
 455 11B the AirCore has now three sections, from the open to the closed end, first 30.1 m of 1/4",  
 456 then 52.1 m of 1/8", and 10.1 m of 1/4" diameter, which we will call "1/4 - 1/8 - 1/4". This was  
 457 done solely to illustrate clearly the effects of using different diameters. Similar to what we saw in  
 458 Fig. 10A, the spread of mixing steepens near the closed end. Also those samples resided not long  
 459 enough in the 1/8" section to have much benefit in terms of slowing down the mixing, but  
 460 between 0.80 and 0.85 they had been long enough in the 1/8" section to have experienced less  
 461 mixing than air ending up at the 0.57 point, the first transition between 1/4 and 1/8".

462 We will now express the amount of spreading (in both directions – twice the rms distance) of  
 463 each equal-mass "packet" of air as a fraction of the total mass of air in the tube, assuming that  
 464 the temperature inside the tube has become uniform. If that fraction were 0.01 everywhere in the  
 465 tube there would be slightly less than 100 independent samples in the AirCore. Slightly less  
 466 because the remaining fill air in the back takes up space. Fig. 12 shows a more realistic  
 467 situation. Each sample takes up the same volume, separated by the blue vertical lines, producing  
 468 vertical boxes. If there is almost no mixing, as in the case of the last sample that entered the  
 469 AirCore, the sample almost completely fills the first volume (or box in Fig. 12A), which is  
 470 indicated by the value 1.0 on the y-axis. The red curve centered on the second box has started to  
 471 "leak" some sample into the adjoining boxes. The next samples shown are the 7<sup>th</sup>, 12<sup>th</sup>, and 17<sup>th</sup>.  
 472 For the latter, the sample is just starting to leak into boxes 15 and 19. To plot the start of this  
 473 process correctly, each packet is subdivided into 13 equal portions. Narrow Gaussian spreading,  
 474 slowly increasing further into the tube, is calculated for each portion, and then summed. The  
 475 width of each Gaussian is shown in Fig. 10C as a function of fraction of cumulative mass in  
 476 the tube, and the area of each curve is 1/13 of the area of the box. This produces a constant value  
 477 of 1.0 in the center and only the outer portions reach into the neighboring boxes.

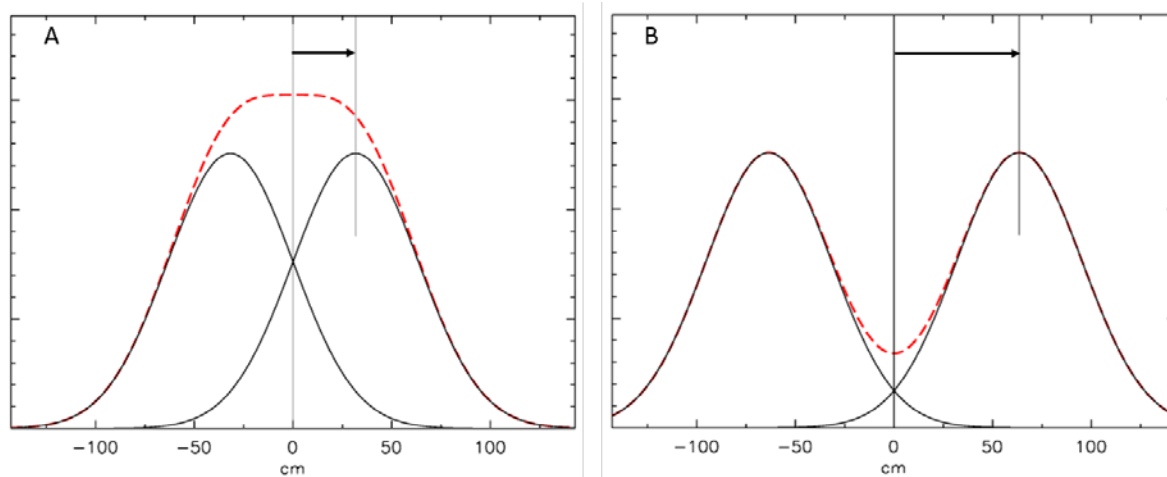


478

479 *Figure 12. A, Mixing of individual air "packets" (red) near the open end with their neighbors*  
 480 *after valve closure for the case shown in Fig. 10C; B, mixing near the closed end (red), vertical*

481 red lines centered on 0.97 show the  $\pm 1 \sigma$  points, black curve is remaining fill air, and the sum of  
482 all actual sample packets, also of those not shown, is the red dashed line.

483 In Fig. 12B we plot the situation near the closed end. As in Fig. 12A, the mixing of only every  
484 fifth air packet is plotted, here ending with the first that came in at the highest altitude, centered  
485 approximately at 0.991. The remaining fill air in this case has the mass of four packets, and the  
486 curves of fill air and of the total air sample (sum of all packets) cross over at exactly the point  
487 where the fourth box from the right starts. How we calculate mixing at a closed end (at  $x = 0$ ) is  
488 shown in Fig. 13.

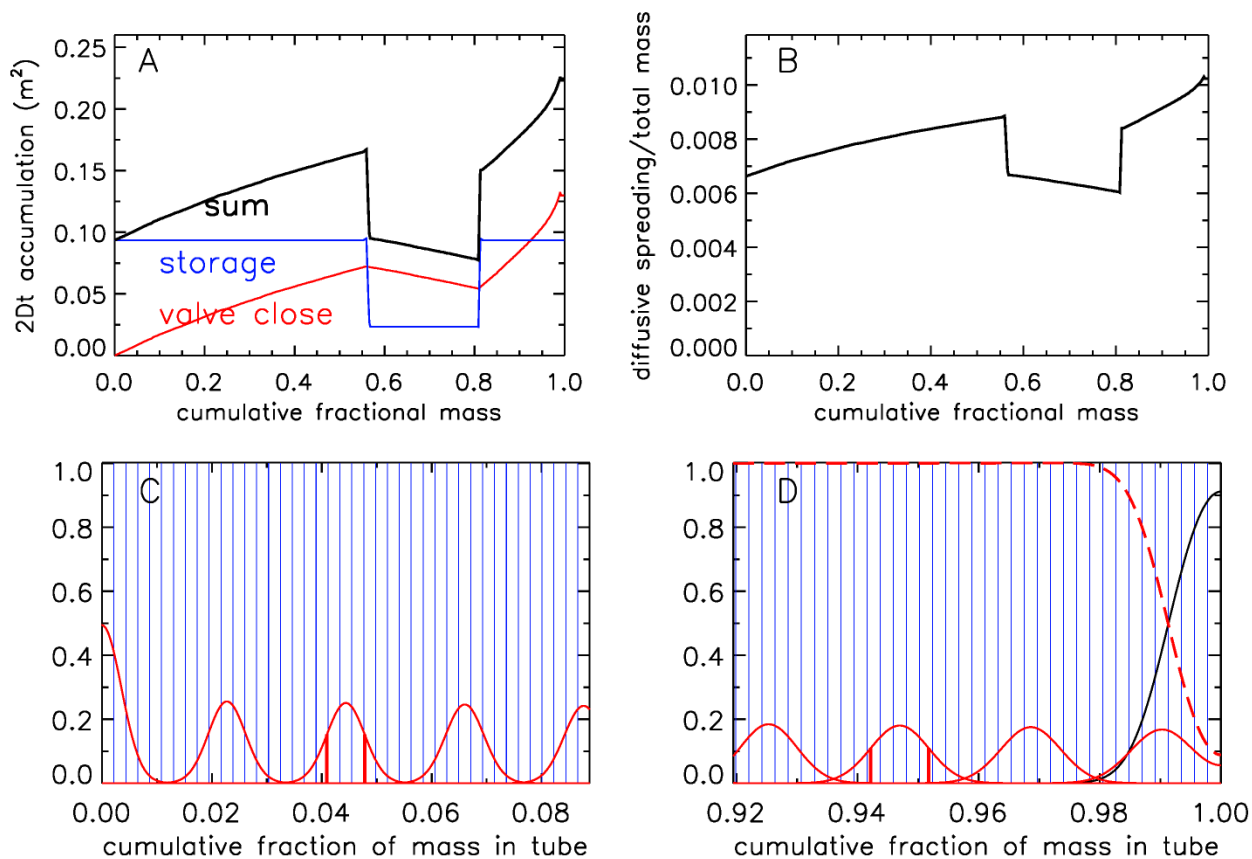


489  
490 *Figure 13. Mixing at a closed end. The Aircore is to the right of the zero centimeter point. A, the*  
491 *distribution of mixing started one hour ago from a plane at 31.8 cm (one root-mean-square of*  
492 *the distribution), indicated by the arrow. A fictitious “mirror” distribution is centered at -31.8*  
493 *cm. The red dashed curve is the sum of the two distributions; B, same calculation, but the center*  
494 *of the distribution is twice as far from the end as in A.*

495 Diffusive mixing that would be to the left of  $x = 0$ , is reflected toward positive values of  $x$ . The  
496 slope of the distribution must be zero at  $x = 0$  because any non-zero slope would imply a  
497 diffusive flux out of, or into, the tube. This is conveniently modeled by assuming a fictitious  
498 distribution mirrored relative to  $x = 0$ , then the two are added, and the portion of the sum for  
499 positive values of  $x$  represents the mixing distribution near a closed end.

500 Let us assume that after the valve has been closed there has been a half hour delay before  
501 analysis starts. Therefore, additional diffusion has taken place, as shown in Fig. 14 for the case  
502  $1/4 - 1/8 - 1/4$  (Fig. 11B). The  $2Dt$  term has been increased by an amount dependent on the  
503 diameter of the tube, normalized as in Eq. 7. In the upper right (panel B) the square root of the  
504 sum has been taken, and then transformed into the spreading width relative to total mass in the

505

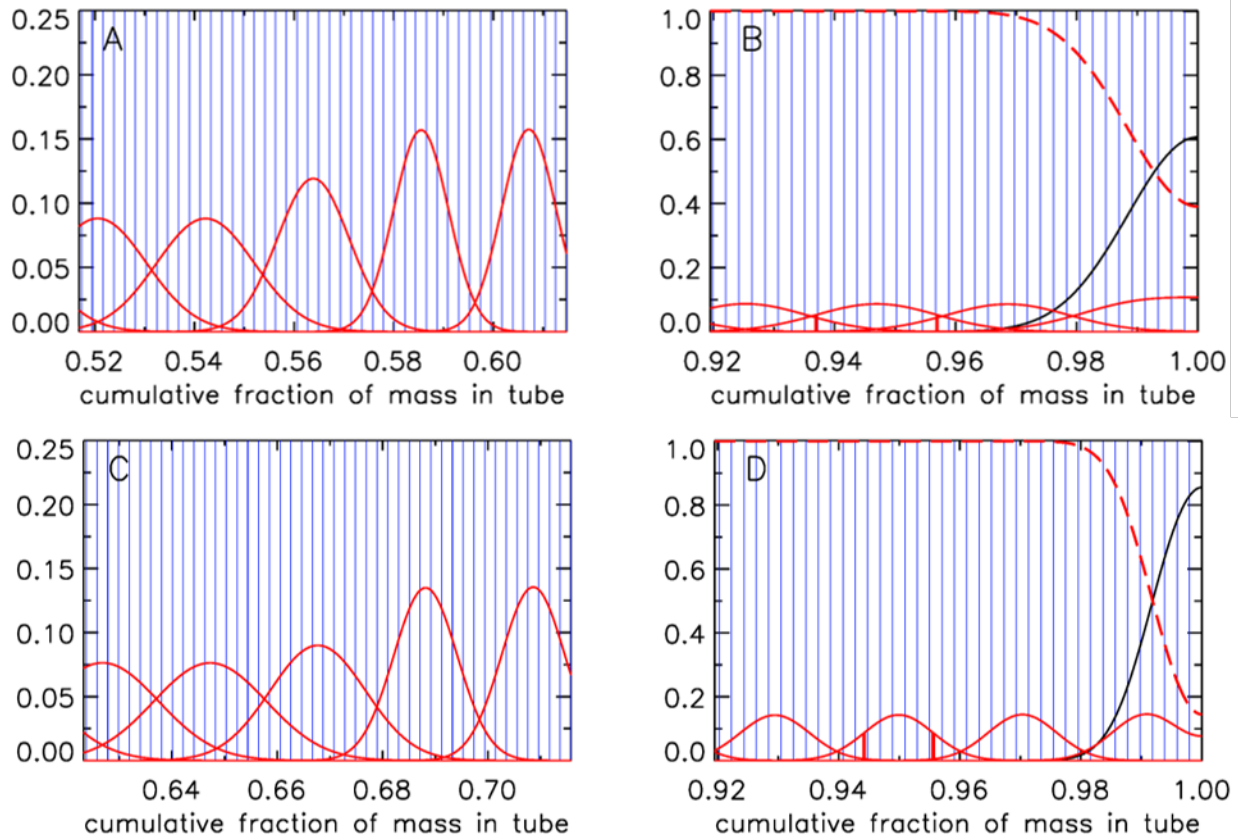


506

507 *Figure 14. Mixing after 30 minutes of storage, for AirCore 1/4 - 1/8 -1/4. A, Sum (black) of the*  
 508 *2Dt accumulation during the flight (red) and during storage (blue), in units of m<sup>2</sup>; B, spreading*  
 509 *width expressed as a fraction of total mass in the tube; C, amount of spreading near what was*  
 510 *the open end, for clarity only every 10<sup>th</sup> packet is shown; D, same, near the closed end. Vertical*  
 511 *red lines show the ±1 σ distances from the peak.*

512 tube. The width is defined here as the distance between the ±1 σ points of the Gaussian which  
 513 contains ~68% of the probability distribution, shown in Fig. 14C at x = 0.0410 and 0.0478  
 514 around the center at x = 0.0444, and in fig. 14D at x = 0.9422 and 0.9518 around the center at x =  
 515 0.9470. These numbers correspond to the full widths shown in fig. 14B. The last packet to enter  
 516 the tube is centered at x = 0.0011 and 1 σ = 0.0033. Most of the diffusive spreading is to the  
 517 right, so that the peak is almost twice as high and the full width a little over half as wide as the  
 518 one centered on x = 0.023.

519 Often the AirCore is analyzed significantly later than 30 min. after valve closure, and the  
 520 measurement process itself may take half an hour. In Fig. 15 the state of mixing four hours  
 521 after valve closure has been calculated, and two AirCore configurations are compared. The



522

523 *Figure 15. Mixing after 4 hours of storage. A, at the transition from 1/4" diameter to 1/8", for*  
 524 *AirCore 1/4 - 1/8 - 1/4; B, near closed end, for 1/4 - 1/8 - 1/4; C, at the transition from 1/4"*  
 525 *diam. to 1/8", for AirCore 1/4 - 1/8; D, near closed end, for 1/4 - 1/8.*

526 spreading width of air “packets” near the closed end is nearly twice as large for the 1/4 - 1/8 –  
 527 1/4 case as for the 1/4 - 1/8 case, and the initial fill air penetrates almost 50% further into the  
 528 tube. It would in most cases not be a good idea to have a wide bore section at the closed end. If  
 529 one waits 24 hours (6 times longer) before starting the analysis, the spreading width near the  
 530 closed end, centered at  $x = 0.9470$ , is 2.32 times larger than after 4 hours, not quite  $\sqrt{6}$  because  
 531 after 4 hours the spreading that occurred during the descent still makes a small, but still  
 532 noticeable, contribution.

533

## 534 7. Potential information content of the AirCore

535 The mixing calculated above allows for a realistic and precise estimate of the altitude resolution  
 536 of the full air sample, both when the AirCore is analyzed in the field promptly after landing, or  
 537 hours or even days later. When the air is slowly pushed through an analyzer, we obtain a quasi-  
 538 continuous curve for the mole fraction of the gases of interest as a function of fractional  
 539 cumulative mass in the tube which is linked to flight data such as pressure altitude, geometric

540 altitude, latitude, longitude, etc. as calculated from the filling dynamics. We define the  
541 information content as the number of independent air samples that are inside the tube, or the  
542 number of degrees of freedom (DoF). Longer wait times before analysis decrease DoF. For  
543 example the small Trainou AirCore (619 cc, Table 1) has DoF of 154, while after waiting four  
544 more hours before analysis DoF has dropped to 67. ~~but it~~ DoF could be decreased further by  
545 additional mixing in the measurement cell, or by successive analyzer cells measuring different  
546 gas species. In the section above we chose more than 400 equal mass packets to calculate  
547 mixing. This was done to prevent a possibly low numerical resolution of the mixing calculation  
548 which would unnecessarily create a low bias in DoF estimates. Ideally, the measurement process  
549 could be modeled in a way similar to the fill and mixing calculation above, convolving the  
550 packets leaving the AirCore with a pulse response of the measurement cell. The response could  
551 be measured separately by introducing a sharp spike just before the cell, and recording how it is  
552 mixed and flushed out. This would be similar to the spiking method described by Wagenhäuser  
553 et al. (2021). In the worst case the measurement cell would be perfectly mixed giving rise to  
554 exponential flushing. In that case, aAfter one cell volume has entered from the AirCore into the  
555 measurement cell, the latter still contains a fraction 1/e of what went through the cell before, so  
556 that the new volume comprises  $(1 - 1/e) = 0.63$  of the cell loading. On the other hand, “plug  
557 flow” (like in the AirCore itself) would produce very little additional mixing, but there could still  
558 be some turbulent eddies near the entrance and exit of the cell. The actual influence of the  
559 measurement cell on mixing lies somewhere in between those two extremes.

560

## 561 8. Numerical implementation

562 The AirCore can consist of one or more sections of different length, each with a different inner  
563 diameter. For example, GML has flown AirCores with a wider bore at the open end and a narrow  
564 bore at the closed end, in order to get better vertical resolution for the stratosphere. The sections  
565 can be divided into a number of smaller segments when Eq. 2 is discretized for numerical  
566 solution (Fig. ~~ure~~ 16):

$$567 \quad Q = -\rho \frac{\pi r^4}{8\eta} \frac{dP}{dz} \Rightarrow Q_j = -\frac{P_j + P_{j+1}}{R(T_j + T_{j+1})} \frac{\pi r_j^4}{8\eta_j} \frac{P_{j+1} - P_j}{dz_j}$$

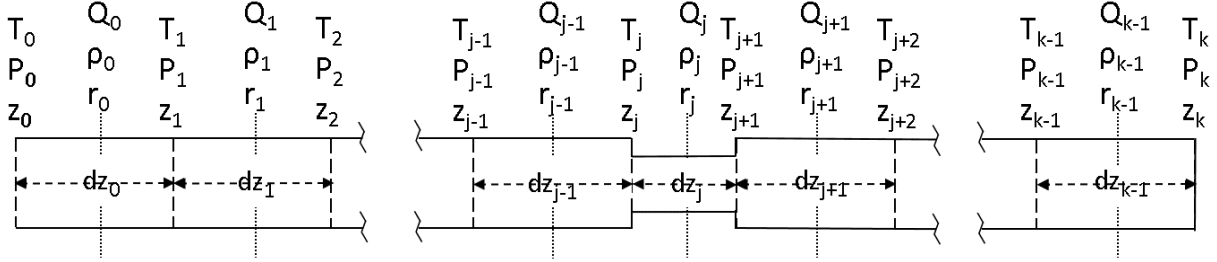
568  $Q_j$  is centered in the middle of segment  $dz_j$ . The first factor in  $Q_j$  is the average amount density  
569 ( $\rho_j$ ). The pressure change at the boundary between segments  $dz_{j-1}$  and  $dz_j$  caused by the  
570 imbalance of the flows  $Q_{j-1}$  and  $Q_j$  is equal to that imbalance divided by the volume between the  
571 mid points of  $dz_{j-1}$  and  $dz_j$ . Adding in the pressure change due to temperature (Eq. 2) we get for  
572 the change at boundary  $j$ :

$$573 \quad \frac{dP_j}{dt} = \frac{P_j}{T_j} \frac{dT_j}{dt} + \frac{T_j}{0.5(dz_{j-1}r_{j-1}^2 + dz_jr_j^2)} \frac{P_j + P_{j+1}}{T_j + T_{j+1}} \frac{r_j^4}{8\eta_j} \frac{P_{j+1} - P_j}{dz_j}$$

574

$$- \frac{T_j}{0.5(dz_{j-1}r_{j-1}^2 + dz_jr_j^2)} \frac{P_{j-1} + P_j}{T_{j-1} + T_j} \frac{r_{j-1}^4}{8\eta_{j-1}} \frac{P_j - P_{j-1}}{dz_{j-1}} \quad \text{Eq. 8}$$

575



576

577 *Figure 16. Coordinate system in the AirCore. The coordinate along the length of the tube is  $z$  (m).*  
 578 *There are  $k$  segments, starting from the open end at  $z_0$  to the closed end at  $z_k$ , between the*  
 579 *vertical dashed lines. Amount flow ( $Q_n$ , mol  $s^{-1}$ ), amount density  $\rho_n$  (mol  $m^{-3}$ ), simply written as*  
 580  *$Q$  and  $\rho$  from here on out, are defined in the middle of each segment, pressures ( $P$ ) and*  
 581 *temperatures ( $T$ ) are defined at the borders of each segment. The length ( $dz$ ) as well as radius*  
 582 *( $r$ ) of the segments may differ.*

583 The first term  $(P/T)(dT/dt)$  is handled separately from the two other terms describing the amount  
 584 change. We write the latter two with the time step going from  $n$  to  $n+1$  (superscript):

$$P_j^{n+1} - P_j^n = \left[ \frac{2T_j^n (P_{j+1}^n + P_j^n)}{T_{j+1}^n + T_j^n} \frac{r_j^4}{\eta_j} \frac{P_{j+1}^{n+1} - P_j^{n+1}}{dz_j} - \frac{2T_j^n (P_{j-1}^n + P_j^n)}{T_{j-1}^n + T_j^n} \frac{r_{j-1}^4}{\eta_{j-1}} \frac{P_j^{n+1} - P_{j-1}^{n+1}}{dz_{j-1}} \right] \frac{t^{n+1} - t^n}{8(dz_{j-1}r_{j-1}^2 + dz_jr_j^2)} \quad \text{Eq. 9}$$

587 On the right hand side we have defined the pressure *differences* at the *end* of the time step. The  
 588 reason is to make the solution of the matrix equation described below unconditionally stable.  
 589 This method has been described as “fully implicit” or “backward time” (Press, 1992). We leave  
 590 the pressure and temperature *averages* as defined at the start of the time step. They determine the  
 591 average amount density of the air and do not create any numerical instability. Eq. 9 can be  
 592 further re-arranged, for  $j=1$  to  $k-1$ , as

$$P_j^n = - \frac{t^{n+1} - t^n}{8(dz_{j-1}r_{j-1}^2 + dz_jr_j^2)} \left[ \frac{2T_j^n (P_{j+1}^n + P_j^n)}{T_{j+1}^n + T_j^n} \frac{r_j^4}{\eta_j dz_j} \right] P_{j+1}^{n+1} +$$

593

$$\begin{aligned}
594 \quad & \left( 1 + \frac{t^{n+1} - t^n}{8(dz_{j-1}r_{j-1}^2 + dz_j r_j^2)} \right) \left[ \frac{2T_j^n(P_{j+1}^n + P_j^n)}{T_{j+1}^n + T_j^n} \frac{r_j^4}{\eta_j dz_j} + \frac{2T_j^n(P_{j-1}^n + P_j^n)}{T_{j-1}^n + T_j^n} \frac{r_{j-1}^4}{\eta_{j-1} dz_{j-1}} \right] P_j^{n+1} \\
595 \quad & - \frac{t^{n+1} - t^n}{8(dz_{j-1}r_{j-1}^2 + dz_j r_j^2)} \left[ \frac{2T_j^n(P_{j-1}^n + P_j^n)}{T_{j-1}^n + T_j^n} \frac{r_{j-1}^4}{\eta_{j-1} dz_{j-1}} \right] P_{j-1}^{n+1} \quad \text{Eq. 10}
\end{aligned}$$

596 This is a tridiagonal matrix equation,  $\mathbf{A} \cdot \mathbf{P}^{n+1} = \mathbf{P}^n$ , linking the  $k+1$  dimensional pressure vector  
597  $\mathbf{P}^{n+1}$  at the end of the time step to the pressure vector  $\mathbf{P}^n$  at the start of the time step. The solution  
598 is  $\mathbf{P}^{n+1} = \mathbf{A}^{-1} \cdot \mathbf{P}^n$ , in which  $\mathbf{A}^{-1}$  is the inverse matrix calculated by the subroutine TRISOL which is  
599 the IDL version of TRIDAG described by Press et al (1992). If the tube is closed at  $z = 0$ , then in  
600 the first line of  $\mathbf{A}$  the first (diagonal) and second (above the diagonal) element (all others are  
601 zero) are respectively

$$602 \quad 1 + \frac{t^{n+1} - t^n}{8(dz_0 r_0^2)} \frac{2T_1^n(P_1^n + P_0^n)}{T_1^n + T_0^n} \frac{r_0^4}{\eta_0 dz_0} \quad \text{and} \quad - \frac{t^{n+1} - t^n}{8(dz_0 r_0^2)} \frac{2T_1^n(P_1^n + P_0^n)}{T_1^n + T_0^n} \frac{r_0^4}{\eta_0 dz_0}$$

603 If the tube is open at  $z = 0$ , then the first element of the first line equals 1, and all others are zero.  
604 In this case  $P_0$  is defined at all times by the outside atmospheric pressure, or by a defined  
605 pressure from a cylinder. There is no influence from any place inside the tube. The algorithm  
606 also allows the other end to be either closed or open to outside air. If closed, then the last two  
607 elements of the  $(k+1)^{\text{st}}$  row are respectively

$$\begin{aligned}
608 \quad & - \frac{t^{n+1} - t^n}{8(dz_{k-1}r_{k-1}^2)} \frac{2T_{k-1}^n(P_{k-1}^n + P_k^n)}{T_{k-1}^n + T_k^n} \frac{r_{k-1}^4}{\eta_{k-1} dz_{k-1}} \quad \text{and} \\
609 \quad & 1 + \frac{t^{n+1} - t^n}{8(dz_{k-1}r_{k-1}^2)} \frac{2T_{k-1}^n(P_{k-1}^n + P_k^n)}{T_{k-1}^n + T_k^n} \frac{r_{k-1}^4}{\eta_{k-1} dz_{k-1}}
\end{aligned}$$

610 If both sides are open, each with a different defined constant pressure, then after an initial  
611 transient the flow settles to steady state flow corresponding to Poiseuille's equation.

612 This describes the core algorithm, of which there are two versions, called tubeflowstep3.pro and  
613 tubeflowstep3Cv.pro. They have been programmed in Interactive Data Language (IDL). These  
614 algorithms have the flexibility to accommodate segments of the tube that have different lengths  
615 as well as diameters, flows in both directions, one or two valves open, a temperature gradient  
616 along the tube with its corresponding viscosity gradient, and variable time steps. Another  
617 routine, called analyzefill\_Gaus\_ict.pro, reads the lengths and diameters of tube sections, valves  
618 and dryer, and the relevant flight data, namely outside air pressure and temperature, the  
619 temperature of the AirCore at different locations along the tube, all as a function of time. If  $C_v$  and  
620  $X_{TPR}$  values of valves are defined they will be used. In that case tubeflowstep3Cv.pro nudges  
621 the apparent internal diameter of one or more valves for a given flow toward satisfying Eq. 5 (see  
622 section 5). This needs to be iterated because when we change the internal valve diameter the  
623 pressures and flows will then adjust elsewhere in the tube. The analyzefill\_Gaus\_ict program

624 also reads altitude, latitude, and longitude, but they are not needed for the flow dynamics  
625 calculation per se. Analyzefill\_Gaus\_ict also sets up the coordinate system and initializes  
626 variables. By calling tubeflowstep3.pro at every time step, or tubeflowstep3Cv.pro if  $C_v$  and  
627  $X_{TPR}$  values are defined, it calculates the pressure in the tube, the amount of air and the amount  
628 flow, and the flow velocity, all as a function of time and location in the tube. This is how  
629 altitude, pressure altitude, latitude, and longitude are tied to position in the tube. The \_Gauss  
630 portion of the name indicates that Gaussian mixing is used as described in this paper, and \_ict  
631 indicates that the program expects the needed information about the tube and the flight in the  
632 ICARTT format.

633 Although developed simultaneously with analyzefill\_Gaus\_ict.pro for the passively filled  
634 AirCore, the tubeflowstep3Cv program can also be used to model flow when the AirCore is  
635 actively filled with a pump and some form of flow and pressure control. In that case a program  
636 equivalent to analyzefill\_Gaus\_ict.pro would need to be developed.

637 The code in analyzefill\_Gaus\_ict.pro also produces diagnostic graphics showing how the fill  
638 proceeded. In fact, all figures in this paper have been produced by analyzefill\_Gaus\_ict.pro  
639 except for Figs. 9 and 13.

640

#### 641 9. Some recommendations for improvements in the analysis of AirCores

642 Laboratory measurements of the flow properties of valves, as expressed in the flow coefficient  
643  $C_v$  and the terminal pressure drop ratio  $X_{TPR}$ , as well as the flow properties of dryers could be  
644 helpful for further improving dynamics code as described in this paper, and will be especially  
645 helpful for potential revisions of sample altitude assignments of older flights. For dryers,  
646 permeability is a more important property than porosity.

647 The precision of the sample mixing estimates could be improved by laboratory measurements of  
648 the pulse response of analyzers, especially when an AirCore is analyzed quickly in the field  
649 because very little mixing has yet occurred for the air that came in last.

650 In addition to measuring the pressure inside the tube during a flight at the closed end, one could  
651 consider measuring the pressure inside at a place closely behind the valve(s) plus dryer at the  
652 open end. It does not need to be done routinely, but it would give a history of the total pressure  
653 drop across the valve and dryer only.

654 In cases where people want to fly AirCores without a dryer it could be helpful to study wall  
655 effects. Water vapor adheres tightly to many surfaces, and as anyone experienced with vacuums  
656 knows, it is often hard to pry it off the walls. One possible experiment would be to inject a short  
657 pulse of wet air at one end of a thoroughly dried tube and register what comes out at the other  
658 end. How much stays behind, for how long? How does it affect other species? In general, wall



659 effects could make the AirCore into a (poor) gas chromatograph if gases have different  
660 adsorption/desorption properties.

661

## 662 **Acknowledgement**

663 I thank Anna Karion, Colm Sweeney, Tim Newberger, Jack Higgs, Sonja Wolter, and Bianca  
664 Baier of GML for making our lab's AirCore program blossom. Especially the controlled return  
665 on a glider is a very promising improvement over the return by parachute.

666

667 The main flight analysis program and subroutines in the IDL language are available at  
668 <https://gml.noaa.gov/aftp/user/tans/AirCoreIDL/>

669

## 670 **References**

671 Battle, M., M. Bender, T. Sowers, P. Tans, J. Butler, J. Elkins, J. Ellis, T. Conway, N. Zhang, P.  
672 Lang, and A. Clarke (1996), Atmospheric gas concentrations over the past century measured in  
673 air from firn at the South Pole, *Nature* 383, 231-235.

674 Berg, R. (2005), Simple flow meter and viscometer of high accuracy for gases, *Metrologia* 42,  
675 11-23.

676 Chapman, S. and T. Cowling (1970), *The mathematical theory of non-uniform gases*, 3<sup>rd</sup> edition,  
677 Cambridge University Press.

678 Jeans, J. (1952), *An introduction to the kinetic theory of gases*, Cambridge Univ. Press.

679 Kadoya, K., N. Matsunaga, and A. Nagashima (1985), Viscosity and Thermal Conductivity of  
680 Dry Air in the Gaseous Phase, *J. Phys. Chem. Ref. Data* 14, no. 4, 947-970

681 Karion, A., C. Sweeney, P. Tans, T. Newberger (2010), AirCore: An innovative atmospheric  
682 sampling system, *J. Atmos. Oceanic Technology* 27, 1839-1853. doi:  
683 10.1175/2010JTECHA1448.1

684 Lekner, J. (2019), Laminar viscous flow through pipes, related to cross-sectional area and  
685 perimeter length, *Am. J. Phys.* 87, 791, doi: 10.1119/1.5113573

686 Massman, W. (1998), A review of the molecular diffusivities of H<sub>2</sub>O, CO<sub>2</sub>, CH<sub>4</sub>, CO, O<sub>3</sub>, NH<sub>3</sub>,  
687 N<sub>2</sub>O, NO, and NO<sub>2</sub> in air, O<sub>2</sub> and N<sub>2</sub> near STP, *Atmos. Environm.* 32, 1111-1127

688 [Membrive, O., C. Crevoisier, C. Sweeney, F. Danis, A. Hertzog, A. Engel, H. Bönish, and L.](#)  
689 [Picon \(2017\), AirCore-HR: a high resolution column sampling to enhance the vertical](#)  
690 [description of CH<sub>4</sub> and CO<sub>2</sub>, Atmos. Meas. Tech. 10, 2163-2181, doi: 10.5194/amt-10-2163-](#)  
691 [2017](#)

692 Moore, F., E. Ray, K. Rosenlof, J. Elkins, P. Tans, and C. Sweeney (2014), A cost effective trace  
693 gas measurement program for long term monitoring of the stratospheric circulation, Bull. Amer.  
694 Meteor. Soc., 95, 147-155, doi: 10.1175/BAMS-D-12-00153.11G

695 O'Hanlon, J. (1980), A user's guide to vacuum technology, Wiley & Sons, New York, ISBN 0-  
696 471-01624-1

697 Press, W., S. Teukolski, W. Vetterling, and B. Flannery (1992), Numerical Recipes in Fortran,  
698 2<sup>nd</sup> Edition, Cambridge University Press, ISBN 0-521-43064-X

699 Sevast'yanov, R., and R. Chernyavskaya (1986), Virial coefficients of nitrogen, oxygen, and air  
700 at temperatures from 75 to 2500 K, J. Engineer., Phys. and Thermophys. 51, 851-854.

701 Swagelok (2020), Valve Sizing Technical Bulletin, downloaded September 2020 from  
702 [www.swagelok.com/en/toolbox/cv-calculator](http://www.swagelok.com/en/toolbox/cv-calculator)

703 Tans, P. (2009), System and method for providing vertical profile measurements of atmospheric  
704 gases. U.S. Patent 7,597,014 (6 Oct. 2009)

705 VIM3, International vocabulary of metrology – Basic and general concepts and associated terms,  
706 JCGM 200:2008, published by Bureau International de Poids et Mesures (BIPM).

707 Wagenhäuser, T., A. Engel, R. Sitals (2021), Testing the altitude attribution and vertical  
708 resolution of AirCore measurements with a new spiking method, Atmos. Meas. Techn. 14, 1-12,  
709 doi: 10.5194/amt-14-1-2021.

710

711

712